nature nanotechnology

ARTICLES

https://doi.org/10.1038/s41565-022-01096-2

Cross-species transcriptomic signatures identify mechanisms related to species sensitivity and common responses to nanomaterials

Becky J. Curtis[1], Nicholas J. Niemuth[1], Evan Bennett[1], Angela Schmoldt[2], Olaf Mueller[2], Aurash A. Mohaimani[2], Elizabeth D. Laudadio[3,5], Yu Shen[4], Jason C. White[4], Robert J. Hamers[3] and Rebecca D. Klaper[1,2] ✉

Physico-chemical characteristics of engineered nanomaterials are known to be important in determining the impact on organisms but effects are equally dependent upon the characteristics of the organism exposed. Species sensitivity may vary by orders of magnitude, which could be due to differences in the type or magnitude of the biochemical response, exposure or uptake of nanomaterials. Synthesizing conclusions across studies and species is difficult as multiple species are not often included in a study, and differences in batches of nanomaterials, the exposure duration and media across experiments confound comparisons. Here three model species, *Danio rerio*, *Daphnia magna* and *Chironomus riparius*, that differ in sensitivity to lithium cobalt oxide nanosheets are found to differ in immune-response, iron–sulfur protein and central nervous system pathways, among others. Nanomaterial uptake and dissolution does not fully explain cross-species differences. This comparison provides insight into how biomolecular responses across species relate to the varying sensitivity to nanomaterials.

Engineered nanomaterials (ENMs) exert toxicity towards various organisms, dependent upon physico-chemical properties including surface charge and functionalization, size, shape, and material composition[1]. However, studies have demonstrated up to a 100-fold difference in sensitivity to a given material across species and even cell types studied[1,2]. For example, the half-maximal effective concentration (or EC_{50}) values for the metal oxide nanomaterials copper oxide and zinc oxide range from 0.01 mg l^{-1} in crustaceans to 1.36 mg l^{-1} in fish and 38 mg l^{-1} in protozoa[3]. A mechanistic explanation for this variation across species is unclear, although it could be due to differences in the severity of impact from a common toxicity mechanism (for example, a greater change in oxidative stress pathway indicating pathway disruption).

Variations could also arise from the induction of putative species-specific biochemical mechanisms; however, it is unclear from previous studies whether these mechanisms are really species-specific or were simply the focus of a particular study and not targeted for measurement in others. For example, widely studied silver nanoparticles have been shown to exert a variety of mechanisms of toxicity across different species: these include dysfunctional ion binding, ribonucleic acid (RNA) polymerase and protein metabolism in *Daphnia magna* (daphnids);[4] and oxidative stress in redworms[5]. Concerted efforts are needed to examine multiple species in a uniform manner to identify species-specific mechanisms of ENM toxicity that could lead to sensitivity or, alternatively, species vary in their degree of response of common unifying mechanisms, leading to sensitivity.

Differences in uptake and toxicokinetics may also influence species sensitivity. Alternative feeding strategies could lead to differences in interaction with and uptake of chemicals across species. In addition, particles in aqueous environments may aggregate and interact with environmental constituents such as organic matter, leading to uneven particle distributions in aquatic compartments (for example, benthic versus pelagic) and influencing routes of exposure and bioavailability. For example, benthic-dwelling species tend to be exposed to and ingest a wide range of particle sizes as they aggregate and settle to the benthos, whereas smaller particles are ingested by pelagic daphnids[6].

The current study compares the biochemical responses to sublethal exposures (1 and 10 mg l^{-1}) of lithium cobalt oxide (LCO) nanosheets alongside ion and media controls across model freshwater organisms *D. magna* (daphnids), *Danio rerio* (zebrafish) and *Chironomus riparius* (chironomids). These species represent three taxonomic classes, benthic versus pelagic habitats and different feeding strategies, and have exhibited varying responses to LCO nanosheets in our previous studies. Daphnids are planktonic filter-feeders and have been demonstrated to ingest micrometre- to nano-sized particulates[7]. Omnivorous zebrafish forage heavily in the water column, but also feed from the surface and benthic zones[8]. Larval chironomids are benthic-dwelling detritivores that survive in polluted environments[9]. In our previous work, daphnids exposed to 0.1–25 mg l^{-1} LCO nanosheets exhibited impacts to survival and reproduction starting at 0.25 mg l^{-1} (ref. [10]), zebrafish embryos exhibited significant impacts to gene expression related to oxidative stress and cell death and survival at 1 mg l^{-1} LCO (R.D.K. laboratory, unpublished observations), whereas chironomids exposed to 1, 10 and 100 mg l^{-1} LCO exhibited stunted larval growth, developmental delays, haemoglobin biosynthesis disruptions and impacts to survival starting at 10 mg l^{-1} (ref. [11]).

Nanomaterial toxicity studies often focus on single-species impacts. Comparisons of responses across species have been attempted through the aggregation of information from multiple

[1]School of Freshwater Sciences, University of Wisconsin-Milwaukee, Milwaukee, WI, USA. [2]Great Lakes Genomics Center, University of Wisconsin-Milwaukee, Milwaukee, WI, USA. [3]Department of Chemistry, University of Wisconsin-Madison, Madison, WI, USA. [4]Connecticut Agricultural Experiment Station, New Haven, CT, USA. [5]Present address: Argonne National Laboratory, Lemont, IL, USA. ✉e-mail: rklaper@uwm.edu

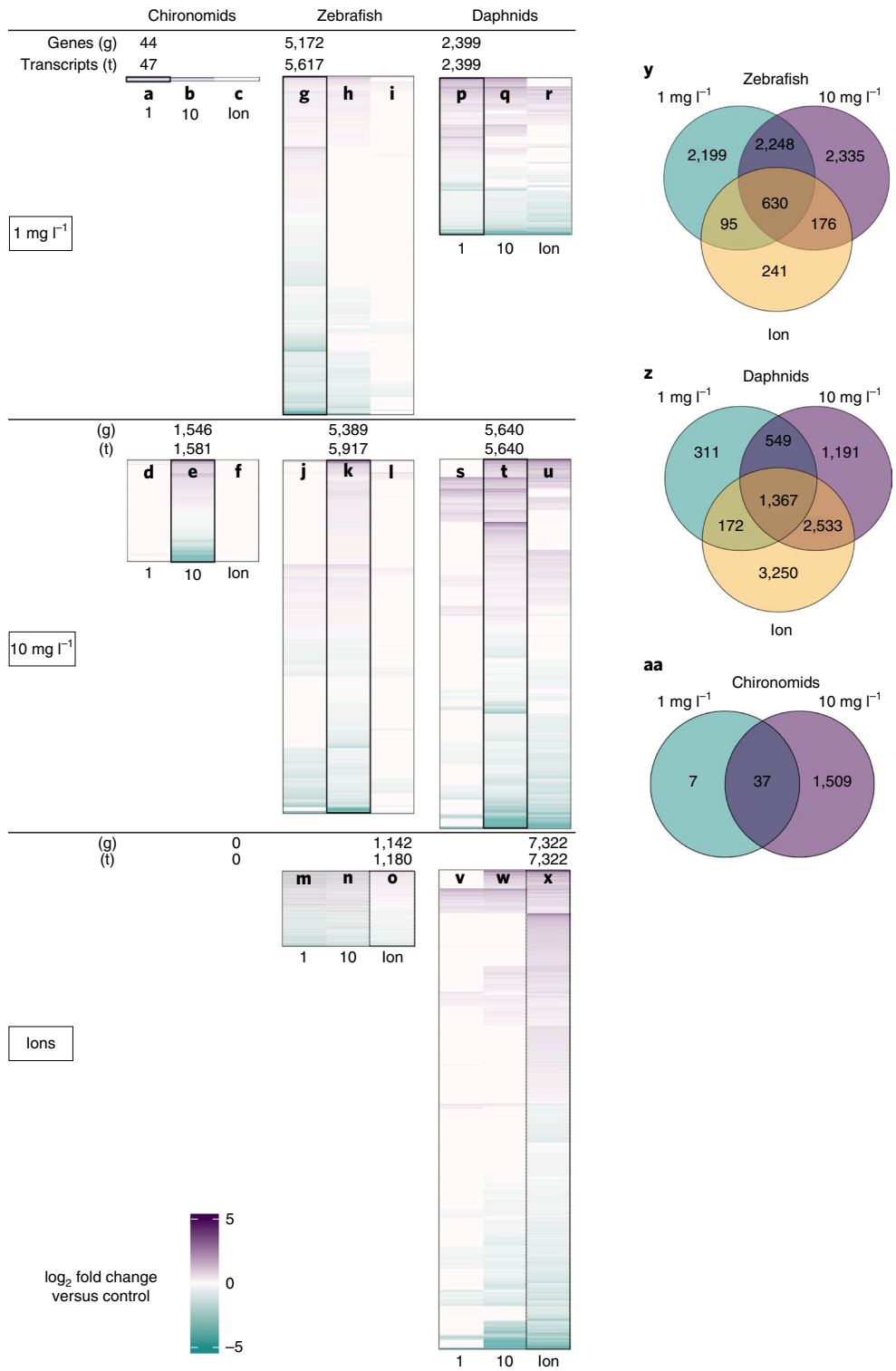

Fig. 1 | Differential gene expression. a–x, Differential expression (versus control, $P_{adj} < 0.05$) across species after exposure to 1 mg l^{-1} LCO nanosheets (**a**,**g**,**p**), 10 mg l^{-1} LCO nanosheets (**e**,**k**,**t**) and an ion control (**o**,**x**). Boxed heatmap column sections (annotated with numbers of DE genes and transcripts) represent differential expression of organisms exposed to the boxed treatment type, while unboxed column sections (**b**,**c**,**h**,**i**,**q**,**r**,**d**,**f**,**j**,**l**,**s**,**u**,**m**,**n**,**v**,**w**) represent corresponding expression patterns in response to other treatments. Each cluster of triplicate columns represents a unique set of genes/transcripts. **y–aa**, Venn diagrams illustrating overlap of DE genes ($P_{adj} < 0.05$) versus control for each species (zebrafish (**y**), daphnids (**z**) and chironomids (**aa**)) and treatment (1 mg l^{-1} LCO (teal), 10 mg l^{-1} LCO (purple) and ion control (yellow)).

studies[12], but this strategy is confounded by non-uniform exposure media, nanomaterial batch effects, different exposure durations and variation in the species' developmental stages. Standardized investigations of ENM–biological interactions have been proposed to generate information that is comparable across different organisms[13]. The current work coordinates the exposure media and dura-

Table 1 | Species-specific pathway disruption

Pathway disruption indicated by DE genes (versus control)	1 mg l^{-1}		10 mg l^{-1}		Ions	
	Z	D	Z	D	Z	D
Blood coagulation (P00011)	X		X			
2-Arachidonoylglycerol biosynthesis (P05726)	X		X			
Androgen/oestrogen/progesterone biosynthesis (P02727)	X		X		X	
Methylcitrate cycle (P02754)				X		
Triacylglycerol metabolism (P02782)	X		X			X
Phenylethylamine degradation (P02766)	X		X		X	
JAK/STAT signalling pathway (P00038)	X		X			X
MYO signalling pathway (P06215)		X		X		X
ALP23B signalling pathway (P06209)		X		X		X
BMP/activin signalling pathway, *Drosophila* (P06211)		X		X		X
DPP signalling pathway (P06213)		X		X		X
GBB signalling pathway (P06214)		X		X		X
SCW signalling pathway (P06216)		X		X		X
Activin beta signalling pathway (P06210)		X		X		X
DPP-SCW signalling pathway (P06212)		X		X		X
Adenine and hypoxanthine salvage pathway (P02723)	X		X			
Alanine biosynthesis (P02724)			X			
Histamine synthesis (P04387)		X		X		X
Cobalamin biosynthesis (P02735)				X		X
Ascorbate degradation (P02729)		X		X		X
Flavin biosynthesis (P02741)		X		X		X
Mannose metabolism (P02752)		X				X
Lipoate biosynthesis (P02750)		X				X
Arginine biosynthesis (P02728)		X				
Succinate to proprionate conversion (P02777)		X				X
Proline biosynthesis (P02768)		X				X
Toll pathway, *Drosophila* (P06217)	X					
Axon guidance mediated by netrin (P00009)	X					
Pyridoxal-5-phosphate biosynthesis (P02759)	X					
Ornithine degradation (P02758)	X					X
O-antigen biosynthesis (P02757)	X					X
N-Acetylglucosamine metabolism (P02756)	X					X
Methylcitrate cycle (P02754)	X					X
Methionine biosynthesis (P02753)	X					X
Histidine biosynthesis (P02747)	X					
Formyltetrahydroformate biosynthesis (P02743)	X					X
Tetrahydrofolate biosynthesis (P02742)	X					
TCA cycle (P00051)	X					
De novo pyrimidine ribonucleotide biosynthesis (P02740)	X					
Plasminogen activating cascade (P00050)	X				X	
De novo pyrimidine deoxyribonucleotide biosynthesis (P02739)	X					
De novo purine biosynthesis (P02738)	X					
Coenzyme A biosynthesis (P02736)	X					X
Allantoin degradation (P02725)	X					
Interferon-γ signalling pathway (P00035)	X					
Xanthine and guanine salvage pathway (P02788)	X					
Vitamin B_6 metabolism (P02787)	X				X	

Continued

Table 1 | Species-specific pathway disruption(Continued)

Pathway disruption indicated by DE genes (versus control)	1 mg l^{-1}		10 mg l^{-1}		Ions	
	Z	D	Z	D	Z	D
Acetate utilization (P02722)	X					X
ATP synthesis (P02721)	X					X
Valine biosynthesis (P02785)	X					
Tyrosine biosynthesis (P02784)	X					
Vitamin D metabolism and pathway (P04396)	X					
Thiamin metabolism (P02780)	X					
p53 pathway feedback loops 1 (P04392)	X					
Glycolysis (P00024)	X					
FAS signalling pathway (P00020)	X					
S-Adenosylmethionine biosynthesis (P02773)	X					
Pyruvate metabolism (P02772)	X					
Pyridoxal phosphate salvage pathway (P02770)	X				X	
Circadian clock system (P00015)	X					X
Cholesterol biosynthesis (P00014)	X					
Glutamine to glutamate conversion (P02745)					X	
Nicotine pharmacodynamics pathway (P06587)						X
Endogenous cannabinoid signalling (P05730)						X
Serine glycine biosynthesis (P02776)						X
Pentose phosphate pathway (P02762)						X
Methylmalonyl pathway (P02755)						X
Lysine biosynthesis (P02751)						X
Leucine biosynthesis (P02749)						X
Isoleucine biosynthesis (P02748)						X
mRNA splicing (P00058)						X
Cysteine biosynthesis (P02737)						X
Asparagine and aspartate biosynthesis (P02730)						X
GABA synthesis (P04384)						X
Aminobutyrate degradation (P02726)						X
5-HT1-type receptor-mediated signalling pathway (P04373)						X
5-HT degradation (P04372)						X
5-HT biosynthesis (P04371)						X
Heterotrimeric G-protein signalling pathway, rod outer segment phototransduction (P00028)						X
General transcription regulation (P00023)						X
General transcription by RNA polymerase I (P00022)						X
DNA replication (P00017)						X
Totals	42	16	8	13	6	48

Indicated by DE genes versus control ($P_{adj} < 0.05$) for both zebrafish (Z) and daphnids (D) exposed to 1 and 10 mg l^{-1} LCO nanosheets and to ions. JAK, Janus kinase; STAT, signal transducer and activator of transcription; MYO, myoglianin; ALP23B, activin-like protein at 23B; BMP, bone morphogenetic protein; DPP, decapentaplegic; GBB, glass bottom boat; SCW, screw; TCA, tricarboxylic acid; ATP, adenosine triphosphate; p53, tumour-suppressor protein; mRNA, messenger RNA; GABA, γ-aminobutyric acid; 5-HT, 5-hydroxytryptamine; DNA, deoxyribonucleic acid.

tion; the nanomaterial and source; and developmental stages across species. Global transcriptomic analysis was used to provide a sensitive molecular analysis of differences and similarities across species that may lead to the measured apical outcomes and identify new mechanisms of action. LCO was chosen as a model transition metal oxide nanomaterial that is widely used in lithium-ion batteries as a cathode material[14]. Considering the meteoric rise in the production of electronics including electric vehicles, and the lack of a national recycling infrastructure for lithium-ion batteries[15], it is reasonable to expect the entry of spent battery waste into aquatic systems.

Finally, differences in body burden were measured to better understand the relationship between uptake and response. Findings from this study expand current knowledge about mechanisms of toxicity exerted by ENMs, providing fresh insight for the refinement or development of new adverse outcome pathways.

Results and discussion

Species-specific transcriptome responses associated with sensitivity to engineered nanomaterial exposure. Global transcriptomic analysis of three different species exposed in the same

study under standardized conditions enabled the identification of species-specific responses. Chironomids, which are the least sensitive to LCO exposure, had the lowest number of differentially expressed (DE) genes (44; Fig. 1a,aa). Owing to their sensitivity, daphnids were anticipated to have the greatest change in gene expression. In fact, zebrafish embryos had the greatest change (versus control) in the absolute number of significant DE genes (5,172; Fig. 1g,y) at the lowest nanoparticle concentration (1 mg l^{-1}) in the study and daphnids had 2,399 (Fig. 1p,z), indicating that this number alone does not represent the nature of why daphnids are more sensitive. At 10 mg l^{-1} exposure, numbers of DE genes in daphnids jumped to 5,640 (Fig. 1t,z), whereas in zebrafish the numbers of DE genes did not change substantially (5,389; Fig. 1k,y) although there were many unique genes in zebrafish (2,335) in the 10 mg l^{-1} exposure not represented at 1 mg l^{-1} (Fig. 1y).

More than the sheer numbers of genes, pathways implicated by DE genes indicate how organisms may be impacted in a species-specific manner, providing insight into different mechanisms that could contribute to species sensitivity (Table 1, where X denotes an impacted pathway). Higher numbers of species-specific disrupted pathways were exhibited by zebrafish and daphnids in response to the lowest nanoparticle concentration (that is, 42 and 16, respectively) compared with the number of pathways exhibited at the highest exposure (8 and 13, respectively), possibly indicating that pathways responsible for sensitivity are instigated at lower concentrations and more shared generic stress responses occur at higher exposures. The least sensitive chironomid organisms exhibited no species-specific pathway disruptions at either concentration. Daphnid-specific pathways included several signalling pathways, vitamin metabolism and histamine synthesis. Histaminergic impairment in daphnids has been demonstrated to disrupt normal phototaxis behaviour, the avoidance of UV damage and predation, which are important in daphnids for survival[16]. Vitamin metabolism impacts included the biosynthesis of cobalamin, the essential form of cobalt. A total of eight pathways were disrupted in zebrafish exposed to 10 mg l^{-1} LCO: these involve triacylglycerol metabolism, the phenylethylamine degradation pathway and others not commonly described as being impacted by exposure to nanomaterials—including JAK/STAT signalling, pathways associated with blood coagulation, the synthesis of various sex hormones and 2-arachidonoylglycerol biosynthesis, which is involved in numerous physiological functions central to larval zebrafish survival. Related physiological functions include locomotion, feeding and energy metabolism, the sensing of pain and the regulation of neuro-inflammation[17]. The least sensitive chironomids did not exhibit impacts to any pathways in a species-specific manner, regardless of LCO concentration.

Pathways impacted in both daphnids and zebrafish after 10 mg l^{-1} nanoparticle exposure included β-adrenergic receptor signalling activity and angiotensin II-stimulated signalling through G proteins and β-arrestin pathways (Supplementary Table 2). Interference with β-adrenergic signalling has been shown to influence cardiac structure and function in *D. magna*[18]. In addition, the renin–angiotensin system is important for regulating cardiac functions, maintaining blood pressure and circulation, and extracellular-fluid levels[19]. While chironomids were less sensitive to the impacts of LCO, and cobalt uptake varied significantly from daphnids (Supplementary Fig. 4), chironomids shared pathways with both species (Supplementary Table 2). In zebrafish these included pathways related to the plasminogen activating cascade (vascular system), the toll pathway (immune function) and amino acid metabolism, whereas in daphnids these included various metabolic pathways, indicating these pathways may be a more common baseline response across species.

Differential gene expression in shared pathways may be related to species sensitivity. The coordinated analysis of all three species enabled the finding that, although some response mechanisms were shared across all species, they may nonetheless show differences. Species sensitivity may result from differences in the expression of different parts of the same pathway. For example, general stress and oxidative stress responses, commonly documented in ENM exposure[20], were evident across all species. However, while all species exhibited DE genes involved in stress and apoptosis-related pathways, such as MAPK, hypoxia response and p53 pathways (Fig. 2a,c), in the more sensitive daphnids and zebrafish, processes involved in reactive oxygen species detoxification and metabolic processes, cellular redox homeostasis, injury and immune-related responses, and other stress and defense responses were significantly enriched (Benjamini–Hochberg, $P_{adj} < 0.05$). The least sensitive chironomid organisms had a higher percentage of genes expressed that are involved in the regulation of apoptosis (Fig. 2c), which may be adaptive in this species. In addition, chironomids and daphnids exhibited differential expression in pathways related to the biosynthesis of lipoate (Supplementary Table 2), the conjugate base of lipoic acid, which has strong antioxidant properties and has been found to ameliorate oxidative stress symptoms, particularly in rats exposed to metal-based nanoparticles[21].

In our previous work we found that iron–sulfur (Fe–S) proteins, important for many metabolic functions related to growth and metabolism across phyla, are inactivated by LCO nanomaterial exposure in chironomids, resulting in decreased haemoglobin production and stunted metabolism, growth and development[11]. In the current study, all species exhibited impacts to the expression of various Fe–S and related proteins (Fig. 3) as well as the disruption of pathways involved in haemoglobin biosynthesis (Fig. 2i). However, a relatively high percentage of DE genes were involved in Fe–S protein pathways in daphnids compared with the other two species, indicating that Fe–S protein disruption may be particularly important in daphnids and is related to their sensitivity to exposure to LCO ENMs. Haemoglobin regulation plays several critical physiological roles for vertebrates, and in *Chironomus* spp. it is important for metabolizing pollutants and improving their survival in harsh environments;[9] in daphnids, haemoglobin production is a general stress response[22]. The fact that these genes and pathways are indicated in this cross-species analysis as a universal response to exposure to a mixed metal oxide further solidifies the disruption of Fe–S proteins and haemoglobin production as a molecular initiating event. The greater number of genes disrupted along the haem-biosynthesis-related pathways in daphnids, which are the most sensitive species (Fig. 2i), indicates a potential mechanism that determines species sensitivity.

Across all three species, LCO nanosheets disrupted the expression of genes in signalling pathways and those related to stress, injury and immune-related responses, apoptosis, energy production and DNA metabolism (Fig. 2a–e), as well as pathways not commonly implicated by nanomaterial exposure, that is, those associated with cardiovascular-system processes, functions

Fig. 2 | Cross-species pathway impacts. Pathway interferences associated with DE genes (10 mg l^{-1} versus control, $P_{adj} < 0.05$), shown as the percentage of DE genes identified through the PANTHER classification system. The number of total DE genes analysed in PANTHER for each species is shown after the species name. **a**, Stress. **b**, Injury/immune-related. **c**, Apoptosis. **d**, Energy. **e**, DNA metabolism/gene expression. **f**, Cell growth. **g**, Metabolism. **h**, Signalling. **i**, Cardiovascular/circulatory. **j**, Neurological. **k**, Sexual maturation/reproduction. MAPK, mitogen-activated protein kinase; HIF, hypoxia-inducible factor; bZIP, basic leucine zipper; EGF, epidermal growth factor; IGF, insulin-like growth factor; PI3, phosphoinositide 3; CCKR, cholecystokinin receptor; FGF, fibroblast growth factor; PDGF, platelet-derived growth factor; TGF, transforming growth factor; VEGF, vascular endothelial growth factor.

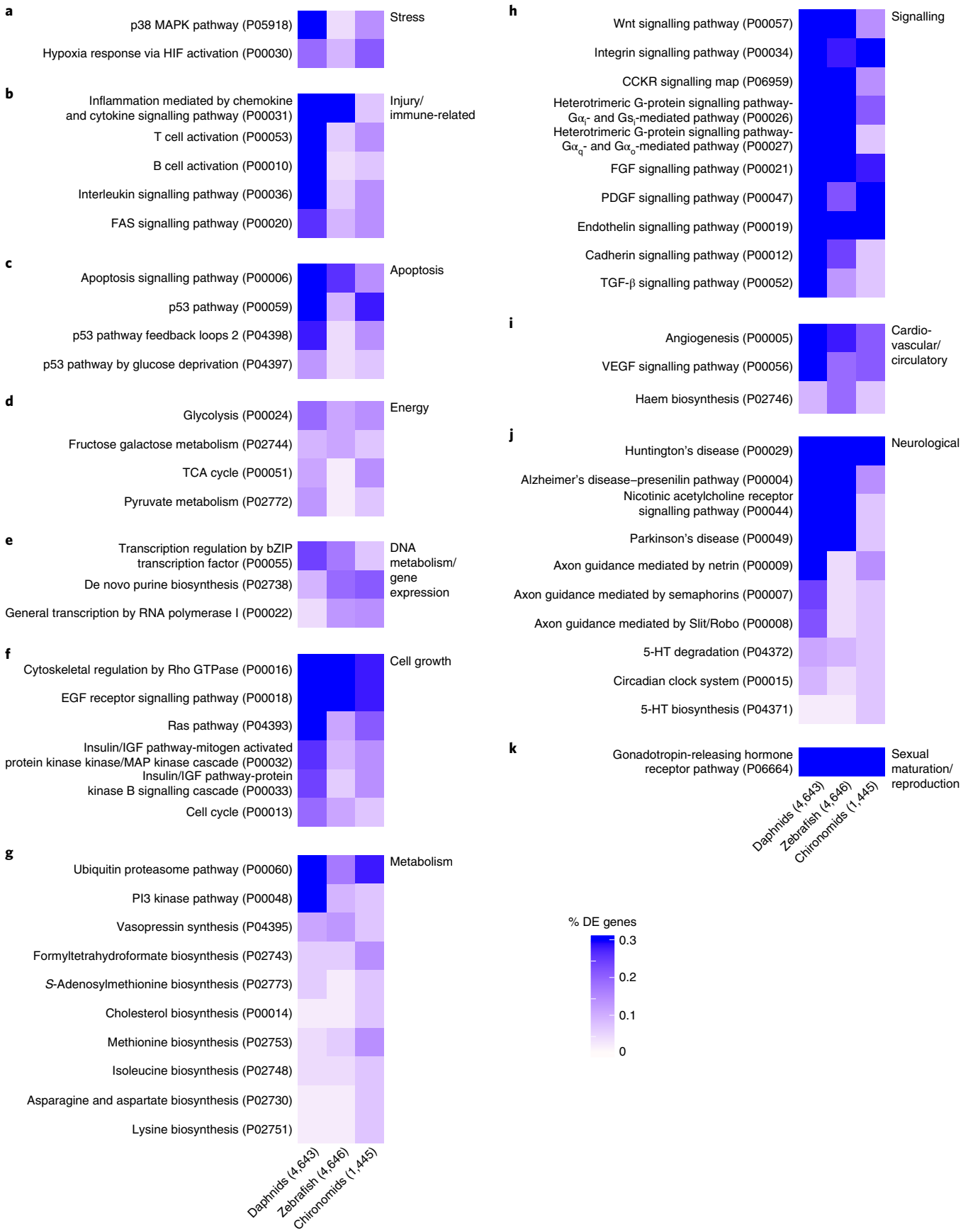
a
p38 MAPK pathway (P05918)
Hypoxia response via HIF activation (P00030)
Stress
b
Inflammation mediated by chemokine and cytokine signalling pathway (P00031)
T cell activation (P00053)
B cell activation (P00010)
Interleukin signalling pathway (P00036)
FAS signalling pathway (P00020)
Injury/ immune-related
c
Apoptosis signalling pathway (P00006)
p53 pathway (P00059)
p53 pathway feedback loops 2 (P04398)
p53 pathway by glucose deprivation (P04397)
Apoptosis
d
Glycolysis (P00024)
Fructose galactose metabolism (P02744)
TCA cycle (P00051)
Pyruvate metabolism (P02772)
Energy
e
Transcription regulation by bZIP transcription factor (P00055)
De novo purine biosynthesis (P02738)
General transcription by RNA polymerase I (P00022)
DNA metabolism/ gene expression
f
Cytoskeletal regulation by Rho GTPase (P00016)
EGF receptor signalling pathway (P00018)
Ras pathway (P04393)
Insulin/IGF pathway-mitogen activated protein kinase kinase/MAP kinase cascade (P00032)
Insulin/IGF pathway-protein kinase B signalling cascade (P00033)
Cell cycle (P00013)
Cell growth
g
Ubiquitin proteasome pathway (P00060)
PI3 kinase pathway (P00048)
Vasopressin synthesis (P04395)
Formyltetrahydroformate biosynthesis (P02743)
S-Adenosylmethionine biosynthesis (P02773)
Cholesterol biosynthesis (P00014)
Methionine biosynthesis (P02753)
Isoleucine biosynthesis (P02748)
Asparagine and aspartate biosynthesis (P02730)
Lysine biosynthesis (P02751)
Metabolism
Daphnids (4,643)
Zebrafish (4,646)
Chironomids (1,445)
h
Wnt signalling pathway (P00057)
Integrin signalling pathway (P00034)
CCKR signalling map (P06959)
Heterotrimeric G-protein signalling pathway-Gαi- and Gαs-mediated pathway (P00026)
Heterotrimeric G-protein signalling pathway-Gαq- and Gαo-mediated pathway (P00027)
FGF signalling pathway (P00021)
PDGF signalling pathway (P00047)
Endothelin signalling pathway (P00019)
Cadherin signalling pathway (P00012)
TGF-β signalling pathway (P00052)
Signalling
i
Angiogenesis (P00005)
VEGF signalling pathway (P00056)
Haem biosynthesis (P02746)
Cardio-vascular/ circulatory
j
Huntington's disease (P00029)
Alzheimer's disease–presenilin pathway (P00004)
Nicotinic acetylcholine receptor signalling pathway (P00044)
Parkinson's disease (P00049)
Axon guidance mediated by netrin (P00009)
Axon guidance mediated by semaphorins (P00007)
Axon guidance mediated by Slit/Robo (P00008)
5-HT degradation (P04372)
Circadian clock system (P00015)
5-HT biosynthesis (P04371)
Neurological
k
Gonadotropin-releasing hormone receptor pathway (P06664)
Sexual maturation/ reproduction
Daphnids (4,643)
Zebrafish (4,646)
Chironomids (1,445)
% DE genes
0.3
0.2
0.1
0

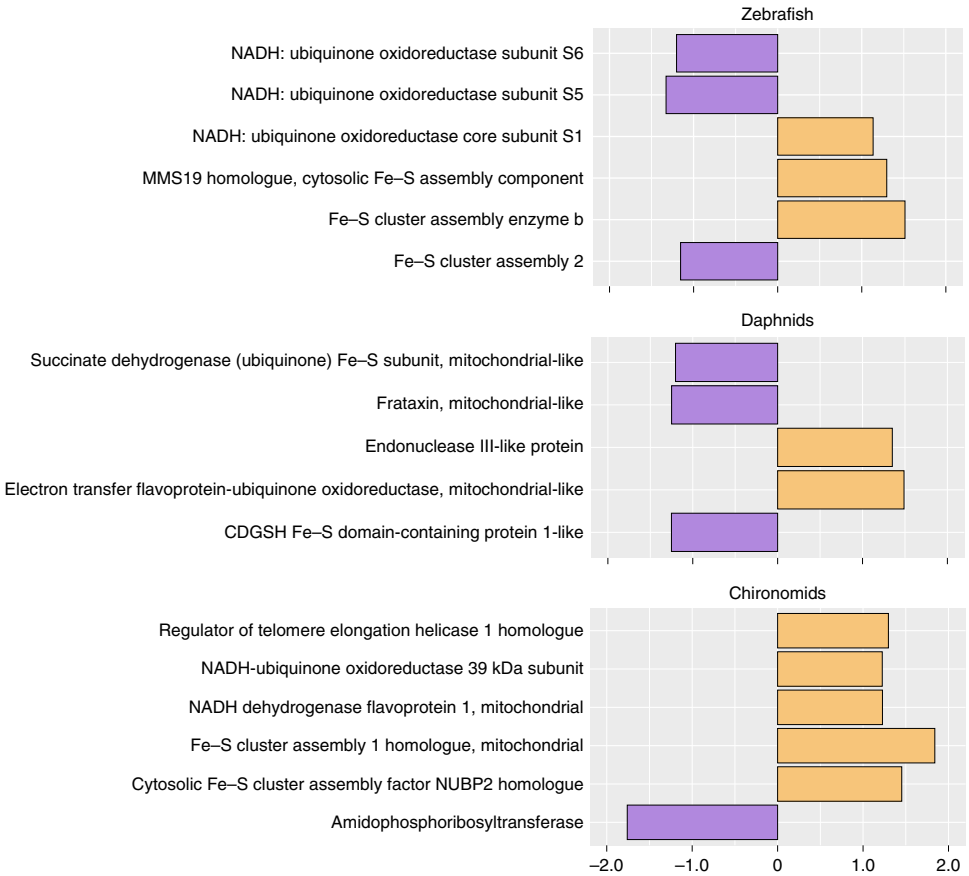

Fig. 3 | Fe–S and related genes. Gene expression for examples of Fe–S and Fe–S-related proteins across species, shown as the fold change versus control after 10 mg l^{-1} nanoparticle exposure. NADH, reduced nicotinamide adenine dinucleotide; MMS19, nucleotide excision repair protein homologue; CDGSH, iron–sulfur binding motif; NUBP2, nucleotide-binding protein 2.

related to the central nervous system, and to sexual maturation and reproduction (Fig. 2i–k; for a full list, see Supplementary Table 2). However, the more sensitive daphnids and zebrafish showed greater enrichment for these pathways, and enrichment was not evident in chironomids.

Several signalling pathways were impacted across all species (Fig. 2h), but zebrafish and daphnids exhibited significant enrichment for processes involved in cellular signalling, indicating that differential expression across species in these pathways could dictate sensitivity. These signalling pathways play important roles in a myriad of biological functions, for example, wingless/integrated (Wnt) signalling, which was impacted and is related to development for both vertebrates and invertebrates[23]. Disruption to cell growth and structure, and to general metabolism pathways were also observed across all species (Fig. 2f,g), with zebrafish and daphnids also exhibiting significant enrichment for these functions. Enriched daphnid gene ontology (or GO) terms included prefoldin complex, which carries out a chaperone role and assists with the proper functioning of actin and tubulin, and is important for homeostasis and contributes to everything from neural development to cytoskeletal structure[24].

Interestingly, several neurological pathways were impacted across the species (Fig. 2j), which is not commonly described as a molecular impact of nanomaterial exposure shared across species. ENM-related disruption of neurological function and circadian rhythm has been suggested for selected species based on behavioural assays, and damage to dopaminergic neurons has been predicted in silico[25]. Disruption of pathways involved with axon guidance mediation, serotonin (5-HT) metabolism and circadian rhythm were observed across all species, as were interferences with pathways associated with neurological malfunction, including Parkinson's, Alzheimer's and Huntington's diseases. Zebrafish and other species have been utilized as models for the study of these diseases[26]. Zebrafish and daphnids shared various enriched central nervous system-related terms, and zebrafish exhibited enrichment for circadian-related terms and those related to neuronal or nervous-system development, which may point to a particular sensitivity in the developing zebrafish embryos.

Significant enrichment of processes related to visual perception and/or abnormalities in eye physiology or morphology were shared in zebrafish and daphnids. The zebrafish genes involved in enriched biological process for protein-folding included subunits of the chaperonin-containing TCP1 gene (CCT) which is associated with several processes including retinal disfunction (*cct2*)[27]; phosducin-like protein, which encodes for phosphoprotein and is expressed in rod cells in the retina[28]; nervous system and hypoxia responses were also enriched.

Alternatively, in some cases, gene expression was similar across species, pointing to more universal responses that did not distinguish sensitivity. For example, numerous energy-production pathways and metabolism, which have been demonstrated in other experiments[29], were impacted across all species (Fig. 2d,g) as were pathways involved in genotoxicity and impacts to DNA metabolism and transcription (Fig. 2e), which have also been demonstrated in other work[30]. In addition, similar percentages of DE genes across all three species indicated disruptions to gonadotropin-releasing hormone receptor activity (Fig. 2k), but zebrafish in particular exhibited enrichment related to hormone secretion and oestrogen response. Hormone disruption presents the potential for impaired

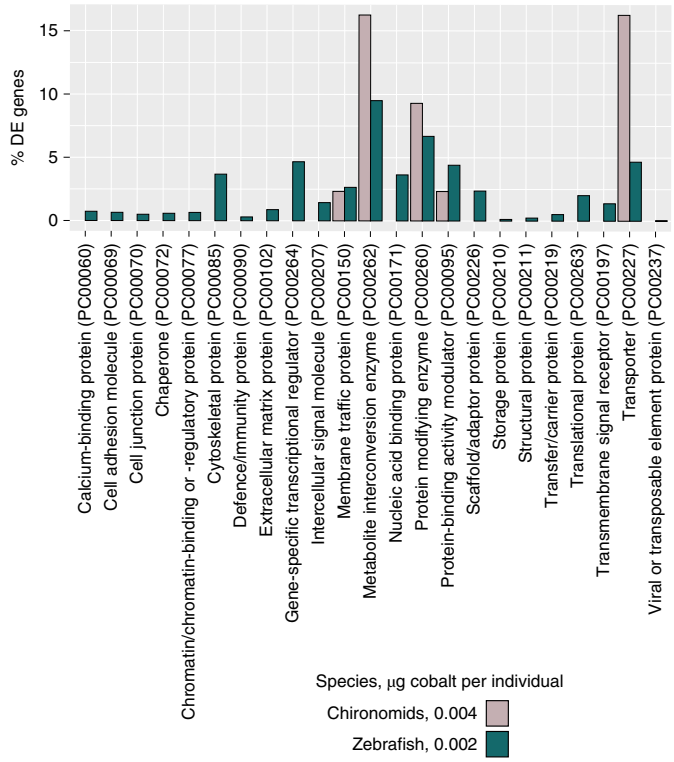

Fig. 4 | Role of uptake, species. Protein classes impacted by exposure of zebrafish (to 10 mg l^{-1} LCO nanosheets) and chironomids (to 1 mg l^{-1} LCO nanosheets), each with similar levels of cobalt uptake. Shown here are the percentages of DE genes identified through PANTHER analysis.

reproductive success, and a growing number of studies have indicated that the consequences of ENM exposure include impacts to the reproductive systems of various organisms[31].

Role of uptake in the molecular impact of nanomaterials. For all species, the number of DE genes increased with increasing cobalt uptake; however, the magnitude of the response was unequal, suggesting that ENM uptake was not the most important driver behind the observed biochemical impacts. At both nanoparticle exposure concentrations, zebrafish exhibited a lower cobalt uptake than chironomids (Supplementary Fig. 4) but were impacted by a much larger number of DE genes ($P_{adj} < 0.05$) at each concentration (5,172 and 5,389, respectively, Fig. 1g,k) than the chironomids (44 and 1,546, respectively, Fig. 1a,e). In addition, zebrafish exposed to 10 mg l^{-1} nanoparticles and chironomids exposed to 1 mg l^{-1} nanoparticles had similar levels of cobalt body burden (0.002 and 0.004 µg cobalt per individual, respectively), yet differential gene expression impact values indicated species-specific impacts on protein classes: chironomids exhibited a stronger impact to metabolite interconversion enzyme and transporter proteins (Fig. 4). Daphnids exhibited the highest cobalt body burden (0.43 and 1.35 µg cobalt per individual, Supplementary Fig. 4) and the largest concentration-dependent increase in DE genes (2,399 versus 5,640 ($P_{adj} < 0.05$), Fig. 1p,t, respectively).

Furthermore, the current work illustrates a distinction between impacts of exposure to nanoparticle formulations and related dissolved ions. Partial least squares discriminant analysis (PLS-DA) indicates that global transcriptomic profiles for ENM- and ion-exposed zebrafish and daphnids show no overlap at either nanoparticle concentration, and chironomid profiles show little overlap between 10 mg l^{-1} and ion profiles (Supplementary Fig. 5, 95% confidence interval). Differential expression in zebrafish exposed to both 10 mg l^{-1} nanoparticle and ions (Fig. 1k,o) were associated with 133 pathways, 30 of which were impacted in a nanoscale-specific manner. Although the patterns of differential expression for transcripts in daphnids exposed to nanoparticles are not the same as those exposed to ions (Fig. 1t versus 1u), nanoscale-specific impacts were not as evident when examining pathway disruption. Of the collective 147 pathways implicated by differential expression in 10 mg l^{-1} particle- and ion-exposed daphnids, only two were impacted in a nanoscale-specific manner. Nonetheless, our previous studies demonstrated nano-specific impacts to survival, reproduction and gene expression for daphnids exposed to LCO nanosheets, which may indicate that global gene-expression responses differ between ion exposures and ENM exposures but the major pathways impacted are the same[10]. Differences across species in the impact of uptake of LCO may be due not only to the biochemistry of the organism but the physiology of the gut of daphnids versus other species. On nanoparticle ingestion, the initial daphnid gut is acidic and could readily lead to particle dissolution and ion release into the anterior gut, as has been shown for silver nanoparticles[32]. Daphnids readily take up the ENMs, and in this study have the highest degree of uptake. This measured uptake could be through ingestion, which is easily seen in the gut of the daphnids, but also due to some adhesion to the carapace, as in the case of other nanoparticles[33]. Adhesion to the carapace may impact daphnid locomotion and cause increased demands to energy budgets. In larval chironomids, nanoparticles have been shown to accumulate in the gut[34], and chironomid species *Chironomus crassicaudatus* has a larval gut pH profile that hovers near neutral (6.7–7.4)[35]. In this environment, metal dissolution would be promoted to a lesser degree than under more acidic conditions. Considering these factors along with the lower rate of ENM uptake by chironomids in this work, dissolution into the gut may occur more slowly and to a lesser degree than in other species, leading to the observed differences in gene-expression patterns. In zebrafish, polystyrene nanoparticles have been shown to translocate to the gut and the eye[36]. In the current work, translocation of the LCO nanosheets to the zebrafish eye could explain the enriched processes in zebrafish related to visual function.

Conclusions

This work provides global transcriptomic insight into impacts of LCO nanosheets across different taxonomic groups in a singular, uniform effort that limits confounding factors by using the same media, nanoparticle source and coordinated developmental stages across the species.

Biomolecular impacts observed in this work revealed species-specific responses to nanomaterials that are associated with sensitivity, both in the number and types of DE genes, and in the pathways impacted with expression. These findings present a wealth of opportunities for further elucidation of how the degree of response of these mechanisms contribute to the variation in responses of ENM toxicity across species.

Changes in pathway disruption unique to more sensitive daphnids and zebrafish indicate that signalling pathways, adrenergic and cardiac-development-related pathways are related to sensitivity. In addition, differences across organisms in gene expression in common pathways related to oxidative stress, Fe–S protein function, neurological function and reproduction may provide evidence of the degree to which these mechanisms relate to species sensitivity. Finally, global transcriptomic response and species-specific physico-chemical characteristics rather than uptake may impact nanoparticle transformation, resulting in changes to nanoparticle bioavailability and toxicity.

The findings of this work have provided insight across several model species of the impacts from ENM exposure that can be further examined to help establish shared biomolecular impacts, dictating the species sensitivity not only to this model ENM but also to others.

Online content

Any methods, additional references, Nature Research reporting summaries, source data, extended data, supplementary information, acknowledgements, peer review information; details of author contributions and competing interests; and statements of data and code availability are available at https://doi.org/10.1038/s41565-022-01096-2.

Received: 25 May 2021; Accepted: 1 February 2022;
Published online: 07 April 2022

References

1. Klaper, R. D. The known and unknown about the environmental safety of nanomaterials in commerce. *Small* **16**, 2000690 (2020).
2. Klaper, R., Arndt, D., Bozich, J. & Dominguez, G. Molecular interactions of nanomaterials and organisms: defining biomarkers for toxicity and high-throughput screening using traditional and next-generation sequencing approaches. *Analyst* **139**, 882–895 (2014).
3. Bondarenko, O. et al. Toxicity of Ag, CuO and ZnO nanoparticles to selected environmentally relevant test organisms and mammalian cells in vitro: a critical review. *Arch. Toxicol.* **87**, 1181–1200 (2013).
4. Hou, J., Zhou, Y., Wang, C., Li, S. & Wang, X. Toxic effects and molecular mechanism of different types of silver nanoparticles to the aquatic crustacean *Daphnia magna*. *Environ. Sci. Technol.* **51**, 12868–12878 (2017).
5. Choi, J. S. & Park, J. W. Molecular characterization and toxicological effects of citrate-coated silver nanoparticles in a terrestrial invertebrate, the earthworm (*Eisenia fetida*). *Mol. Cell. Toxicol.* **11**, 423–431 (2015).
6. Scherer, C., Brennholt, N., Reifferscheid, G. & Wagner, M. Feeding type and development drive the ingestion of microplastics by freshwater invertebrates. *Sci. Rep.* https://doi.org/10.1038/s41598-017-17191-7 (2017).
7. Rist, S., Baun, A. & Hartmann, N. B. Ingestion of micro- and nanoplastics in *Daphnia magna* – quantification of body burdens and assessment of feeding rates and reproduction. *Environ. Pollut.* https://doi.org/10.1016/j.envpol.2017.05.048 (2017).
8. Spence, R., Gerlach, G., Lawrence, C. & Smith, C. The behaviour and ecology of the zebrafish, *Danio rerio*. *Biol. Rev. Camb. Philos. Soc.* **83**, 13–34 (2008).
9. Nath, B. B. Extracellular hemoglobin and environmental stress tolerance in Chironomus larvae. *J. Limnol.* **77**, 104–112 (2018).
10. Bozich, J., Hang, M., Hamers, R. & Klaper, R. Core chemistry influences the toxicity of multicomponent metal oxide nanomaterials, lithium nickel manganese cobalt oxide, and lithium cobalt oxide to *Daphnia magna*. *Environ. Toxicol. Chem.* **36**, 2493–2502 (2017).
11. Niemuth, N. J. et al. Next-generation complex metal oxide nanomaterials negatively impact growth and development in the benthic invertebrate *Chironomus riparius* upon settling. *Environ. Sci. Technol.* **53**, 3860–3870 (2019).
12. Burkard, M., Betz, A., Schirmer, K. & Zupanic, A. Common gene expression patterns in environmental model organisms exposed to engineered nanomaterials: a meta-analysis. *Environ. Sci. Technol.* **54**, 335–344 (2020).
13. Faria, M. et al. Minimum information reporting in bio-nano experimental literature. *Nat. Nanotechnol.* **13**, 777–785 (2018).
14. Wang, X. et al. Improving cyclic stability of lithium cobalt oxide based lithium ion battery at high voltage by using trimethylboroxine as an electrolyte additive. *Electrochim. Acta* **173**, 804–811 (2015).
15. Hamers, R. J. Nanomaterials and global sustainability. *Acc. Chem. Res.* https://doi.org/10.1021/acs.accounts.6b00634 (2017).
16. McCoole, M. D., Baer, K. N. & Christie, A. E. Histaminergic signaling in the central nervous system of *Daphnia* and a role for it in the control of phototactic behavior. *J. Exp. Biol.* **214**, 1773–1782 (2011).
17. Baggelaar, M. P., Maccarrone, M. & van der Stelt, M. 2-Arachidonoylglycerol: a signaling lipid with manifold actions in the brain. *Prog. Lipid Res.* **71**, 1–17 (2018).
18. Jeong, T.-Y. et al. Effect of β-adrenergic receptor agents on cardiac structure and function and whole-body gene expression in *Daphnia magna*. *Environ. Pollut.* https://doi.org/10.1016/j.envpol.2018.06.026 (2018).
19. Margiotta-Casaluci, L., Owen, S. F., Rand-Weaver, M. & Winter, M. J. Testing the translational power of the zebrafish: an inter-species analysis of responses to cardiovascular drugs. *Front. Pharmacol.* **10**, 893 (2019).
20. Mendoza, R. P. & Brown, J. M. Engineered nanomaterials and oxidative stress: current understanding and future challenges. *Curr. Opin. Toxicol.* **13**, 74–80 (2019).
21. Abdelhalim, M. A. K., Qaid, H. A., Al-Mohy, Y. H. & Ghannam, M. M. The protective roles of vitamin E and α-lipoic acid against nephrotoxicity, lipid peroxidation, and inflammatory damage induced by gold nanoparticles. *Int. J. Nanomed.* **15**, 729–734 (2020).
22. Ha, M. H. & Choi, J. Effects of environmental contaminants on hemoglobin gene expression in *Daphnia magna*: a potential biomarker for freshwater quality monitoring. *Arch. Environ. Contamin. Toxicol.* **57**, 330–337 (2009).
23. Prühs, R., Beermann, A. & Schröder, R. The roles of the Wnt-antagonists Axin and Lrp4 during embryogenesis of the red flour beetle *Tribolium castaneum*. *J. Dev. Biol.* **5**, 10 (2017).
24. Liang, J. et al. The functions and mechanisms of prefoldin complex and prefoldin-subunits. *Cell Biosci.* https://doi.org/10.1186/s13578-020-00446-8 (2020).
25. Serra, A. et al. INSIdE NANO: a systems biology framework to contextualize the mechanism-of-action of engineered nanomaterials. *Sci. Rep.* **9**, 179 (2019).
26. Newman, M., Ebrahimie, E. & Lardelli, M. Using the zebrafish model for Alzheimer's disease research. *Front. Genet.* **5**, 189 (2014).
27. Minegishi, Y., Nakaya, N. & Tomarev, S. I. Mutation in the cebrafish *cct2* gene leads to abnormalities of cell cycle and cell death in the retina: a model of CCT2-related Leber congenital amaurosis. *Invest. Ophthalmol. Vis. Sci.* **59**, 995–1004 (2018).
28. Willardson, B. M. & Howlett, A. C. Function of phosducin-like proteins in G protein signaling and chaperone-assisted protein folding. *Cell. Signal.* **19**, 2417–2427 (2007).
29. Wu, D., Ma, Y., Cao, Y. & Zhang, T. Mitochondrial toxicity of nanomaterials. *Sci. Total Environ.* https://doi.org/10.1016/j.scitotenv.2019.134994 (2019).
30. Nel, A. Toxic potential of materials. *Science* **311**, 622–627 (2007).
31. Brohi, R. D. et al. Toxicity of nanoparticles on the reproductive system in animal models: a review. *Front. Pharmacol.* **8**, 606 (2017).
32. Yan, N., Tang, B. Z. & Wang, W.-X. In vivo bioimaging of silver nanoparticle dissolution in the gut environment of zooplankton. *ACS Nano* https://doi.org/10.1021/acsnano.8b06003 (2018).
33. Adam, N., Leroux, F., Knapen, D., Bals, S. & Blust, R. The uptake of ZnO and CuO nanoparticles in the water-flea *Daphnia magna* under acute exposure scenarios. *Environ. Pollut.* **194**, 130–137 (2014).
34. Lorenz, C. S. et al. Nano-sized Al_2O_3 reduces acute toxic effects of thiacloprid on the non-biting midge *Chironomus riparius*. *PLoS One* **12**, e0176356 (2017).
35. Frouz, J., Lobinske, R. J., Yaqub, A. & Ali, A. Larval gut pH profile in pestiferous *Chironomus crassicaudatus* and *Glyptotendipes paripes* (Chironomidae: Diptera) in reference to the toxicity potential of *Bacillus thuringiensis* serovar *israelensis*. *J. Am. Mosq. Control Assoc.* **23**, 355–358 (2007).
36. van Pomeren, M., Brun, N. R., Peijnenburg, W. J. G. M. & Vijver, M. G. Exploring uptake and biodistribution of polystyrene (nano)particles in zebrafish embryos at different developmental stages. *Aquat. Toxicol.* **190**, 40–45 (2017).

Methods

Lithium cobalt oxide nanoparticle synthesis and characterization. Nanoparticles of LCO ($Li_{0.77}CoO_2$) were synthesized as described previously[37] (see Supplementary Information for detailed synthesis methods). Surface area measurements were conducted using the Brunauer–Emmett–Teller method to obtain the surface area value of 130 $m^2 g^{-1}$. Scanning electron microscopy shows sheet-like particles that are imaged edge-on (Supplementary Fig. 1). Previous size analysis using transmission electron microscopy has yielded approximate diameters of 25 nm and widths of 5 nm. Powder X-ray diffraction yields patterns consistent with previously published work that can be indexed to the $R\bar{3}m$ space group (Supplementary Fig. 2). Our previous work has shown that these LCO nanoparticles have a zeta potential of -12.6 ± 0.6 mV at 1 $mg l^{-1}$ and -3.7 ± 0.5 mV at and 10 $mg l^{-1}$ in moderately hard water and a lateral dimension of <100 nm and a thickness of <5 nm[38]. LCO nanomaterials exhibit relatively rapid settling behaviour in aqueous media (particularly in the presence of food): 70% and 90% in two days for 10 $mg l^{-1}$ and 100 $mg l^{-1}$, respectively[11].

LCO nanosheet and ion suspensions. LCO nanosheets (20 $mg l^{-1}$) were suspended in pure water and bath sonicated using a Branson 2800 ultrasonic bath (Emerson Electric) at 21 °C and 100% power before preparing a dilution of 2 $mg l^{-1}$ in pure water. Final exposure media for each of the three organisms were prepared at concentrations of 10 and 1 $mg l^{-1}$ LCO nanosheets that correspond to a range of sublethal toxicities across species from our previous experiments[10,11]. An ion solution containing lithium and cobalt ions was prepared using dissolved lithium and cobalt metal salts (lithium hydroxide and cobalt chloride) at concentrations equivalent to the 48-hour dissolved fraction of 10 $mg l^{-1}$ LCO nanosheets in moderately hard reconstituted water (MHRW): 2.91 $\mu g l^{-1}$ cobalt and 1.6 $\mu g l^{-1}$ lithium[11].

Cultures and organisms. Daphnids were acquired from Aquatic Research Organisms and cultured (20 daphnids per litre) in MHRW prepared according to US Environmental Protection Agency guidelines[39], composed of 60 $mg l^{-1}$ $MgSO_4$, 96 $mg l^{-1}$ $NaHCO_3$, 60 $mg l^{-1}$ $CaSO_4$, 4 $mg l^{-1}$ of KCl and 0.02 $ml l^{-1}$ of $Na_2SeO_3{\cdot}5H_2O$ (added using a 330 $mg l^{-1}$ $Na_2SeO_3{\cdot}5H_2O$ solution). The MHRW was produced at a twofold concentration, aerated for 48 h using an air stone and then diluted with equal parts of ultrapure water. Cultures were maintained at 20 °C under a 16:8 light/dark cycle and fed algae (25 ml; *Raphidocelis subcapitata*, ~500,000 algal cells per ml) and alfalfa suspension (10 ml; 8 g *Medicago sativa* supplement in one litre of Milli-Q water, agitated for 20 min at 130 revolutions per min using a Thermo Scientific MaxQ 4450 orbital shaker). Media changes, feeding and removal of neonates occurred three times per week. Adult wild-type (5D) zebrafish were from a long-term culture at the School of Freshwater Sciences, maintained in a recirculating aquatic habitat under a 16:8 light/dark cycle at approximately 27 ± 2 °C and fed using TetraMin tropical flakes, bloodworms and live *Artemia*. Zebrafish culture maintenance and exposure followed protocols approved by the University of Wisconsin-Milwaukee (UWM) Institutional Animal Care and Use Committee, including (20-21 no. 01 and 20-21 no. 50). Chironomid egg cases were acquired from Aquatic Research Organisms. On hatching, the larvae were fed daily with supernatant (500 µl) from a 20 $mg ml^{-1}$ suspension of crushed and sieved TetraMin tropical flakes and, starting at day 3, with the full suspension (250 µl).

Experimental design. Coordinated exposures for all species were carried out in MHRW at developmental stages equivalent to five days post-feeding commencement: daphnids, five days old; zebrafish larvae, ten days post-fertilization; and chironomid larvae, five days post-hatch. All organisms were exposed for 48 h to one of four treatments: 1 or 10 $mg l^{-1}$ LCO nanosheets or a media or ion control. Non-living food was administered after the addition of nanoparticles to the exposure vessels, that is, daphnids/alfalfa, chironomid larvae/powdered TetraMin tropical flakes, and zebrafish larvae/Golden Pearl 50 µm larval diet. To satisfy burrowing behaviour and natural feeding mechanisms, chironomid exposure vessels contained autoclaved 140-270 mesh silica sand (5 g) from AGSCO, which had been rinsed three times with pure water.

For RNA sequencing, five daphnid replicates included ten daphnids per 10 ml volume, zebrafish included five replicates of twenty zebrafish larvae per 40 ml volume, and chironomids included five replicates of five larvae per 40 ml control or exposure media. Replicates of pooled whole organisms were flash-frozen using liquid nitrogen and stored at −80 °C for subsequent RNA extraction, complementary DNA library creation and next-generation RNA sequencing.

Additional replicates were conducted to determine uptake of nanomaterials. Organisms were set up in exposure vessels as described above. To ensure sufficient tissue for analysis, a single body burden replicate was created by pooling organisms from five replicates (daphnids), ten replicates (chironomids) and four replicates (zebrafish). This pooling method was used to create triplicate (chironomids and daphnids) and quadruplicate (zebrafish) body burden replicates. Pooled larvae were gently rinsed three times with ultrapure water before flash freezing and storage at −80 °C.

Elemental body burden. Samples were shipped on dry ice to the Connecticut Agricultural Experiment Station. Weighed samples were amended with concentrated nitric acid (5 ml) and heated at 115 °C for 45 min using a hot block (DigiPREP System, SCP Science). After dilution to 50 mL, lithium and cobalt contents were quantified via inductively coupled plasma optical emission spectroscopy using an iCAP 6500 system (Thermo Fisher Scientific). The elemental (lithium and cobalt) calibration concentration of the standard was set as follows: 0, 0.1, 1 and 10 $\mu g l^{-1}$, with 10 $\mu g l^{-1}$ ytterbium set as the internal standard. Individual elemental concentrations were calculated as micrograms per gram of the total sample. Each sample was analysed in three technical replicates.

Illumina RNA-Seq library preparation and sequencing. Total RNA was isolated using the standard protocol for the Direct-zol RNA MiniPrep kit (R2051, Zymo Research). Briefly, whole organisms were homogenized in TRIzol reagent using a pestle and a microcentrifuge tube, and RNA was purified using Zymo-Spin IIC columns (Zymo Research). Total RNA purification was assessed using a NanoDrop spectrophotometer, quantification was measured using a Qubit fluorometer, and integrity was measured using an Agilent Bioanalyzer 2100 instrument. Samples with an optical density (OD) ratio for OD_{260}/OD_{280} of 1.8–2.0 and OD_{260}/OD_{230} of 2.0–2.2 and an RNA integrity number (or RIN) of >7 were used. RNA-sequencing libraries were prepared using Illumina TruSeq Stranded mRNA sample preparation kits (RS-122-2102) and IDT for Illumina TruSeq RNA UD Indexes (20022371) following standard protocols, using total RNA (200 ng). All libraries were sequenced using an Illumina NovaSeq 6000 system, with paired-end 150 base-pair reads.

Transcript identification and RNA-Seq analysis. Sequence data were assessed for quality using FastQC v.0.11.5[40], with no apparent base-calling errors needing to be removed. Illumina TruSeq 3′-anchored primers were clipped using Cutadapt v.1.18[41]. For zebrafish, quality-controlled data were pseudoaligned and sample-quantified against the GRCz11 Ensembl release of the zebrafish reference transcriptome, and for *D. magna*, data were pseudoaligned and sample-quantified against the daphmag2.4 Ensembl release of the *D. magna* reference transcriptome, both using Kallisto v.0.45.0[42]. For *C. riparius*, data were de novo assembled into a draft reference transcriptome using Trinity v.2.8.3[43]. The assembly was then iteratively annotated against the set of NCBI proteins affiliated with *C. riparius*, followed by the annotated genome releases for *Anopheles gambiae*, *Culex quinquefasciatus* and *Aedes aegypti*; the UniProt/SwissProt release from February 2019[44] was used as a final annotation target. Annotations were made using the BLASTX aligner within the NCBI-BLAST+ package v.2.2.28[45]. Paired-end data were subsequently pseudoaligned and sample-quantified against the annotated draft reference transcriptome using Kallisto v.0.45.0[42]. Differential expression analysis of sample pairs was performed using the DESeq2 package[46] within R v.3.5.3, and the resulting tables of DE transcripts were re-annotated with each reference and relationally joined with Kallisto sample quantification counts. A recently updated chironomid genome was used for further downstream analysis[47]. See Supplementary Table 1 and Supplementary Fig. 3 for sequencing profiles and DE transcript regulation.

Cross-species transcriptomic response profiles. Global gene expression was analysed using PLS-DA in the R programming language with the mixOmics package[48]. Quality-control screening was carried out on raw read count data for which gene expression was detected in at least 10% of all exposure replicates. Read counts were normalized using variance stabilizing transformation, and hypervariant sequences were filtered out based on coefficients of variation across sample replicates using the Bioconductor R package DaMiRseq[49]. Heat maps of DE genes for each exposure condition versus control ($P_{adj} < 0.05$) were created and hierarchichal clustering was performed using the Bioconductor package ComplexHeatmap[50].

Functional classification and enrichment. Transcripts that were significantly ($P_{adj} < 0.05$) differentially expressed (versus control) for 1 $mg l^{-1}$ LCO-, 10 $mg l^{-1}$ LCO- and ion-exposed organisms were analysed using the PANTHER (protein analysis through evolutionary relationships) classification system, and generic mapping files were created via PANTHER's hidden Markov model (HMM) scoring tool[51] to enable a more comprehensive analysis of the sequencing data for *D. magna* and *C. riparius*, two species that are annotated to a lesser degree than *D. rerio* and are not included in PANTHER's reference genome database. Input data for *D. rerio* consisted of Ensembl gene identities. Comparisons were made across all species exposed; however, no pathways were implicated in the chironomids at 1 $mg l^{-1}$ (see full results in Supplementary Table 2). As pathways obtained through this analysis are not mutually exclusive, functional enrichment of Gene Ontology (GO) and Human Pathology Ontology (HP) classes, and pathway enrichment (Kyoto Encyclopedia of Genes and Genomes and Reactome) were carried out using g:Profiler[52] to identify mechanisms that may dominate the response. Genes significantly ($P_{adj} < 0.05$) differentially expressed versus control were analysed, using a Benjamini–Hochberg false-discovery rate correction and a significance level of $P < 0.05$. Zebrafish and daphnids were analysed using custom statistical domains comprised of quality-controlled globally-detected reads. Chironomids were analysed using the *A. gambiae* reference species as a background, using all known genes as the scope of statistical domain.

Data availability

RNA-sequencing data are accessible through the National Center for Biotechnology Information's Gene Expression Omnibus via accession numbers GSE161036 (chironomids), GSE174016 (daphnids) and GSE179495 (zebrafish).

References

37. Laudadio, E. D., Bennett, J. W., Green, C. M., Mason, S. E. & Hamers, R. J. Impact of phosphate adsorption on complex cobalt oxide nanoparticle dispersibility in aqueous media. *Environ. Sci. Technol.* **52**, 30 (2018).
38. Niemuth, N. J. et al. Protein Fe–S centers as a molecular target of toxicity of a complex transition metal oxide nanomaterial with downstream impacts on metabolism and growth. *Environ. Sci. Technol.* **54**, 15257–15266 (2020).
39. Smith, M. & Lazorchak, J. A reformulated, reconstituted water for testing the freshwater amphipod, *Hyalella azteca*. *Environ. Toxicol. Chem.* **16**, 1229–1233 (1997).
40. Andrews, S. FastQC: a quality control tool for high throughput sequence data. *Babraham Bioinformatics* http://www.bioinformatics.babraham.ac.uk/projects/fastqc/ (2010).
41. Martin, M. Cutadapt removes adapter sequences from high-throughput sequencing reads. *EMBnet J.* **17**, 10–12 (2011).
42. Bray, N. L., Pimentel, H., Melsted, P. & Pachter, L. Near-optimal probabilistic RNA-seq quantification. *Nat. Biotechnol.* **34**, 525–527 (2016).
43. Grabherr, M. G. et al. Full-length transcriptome assembly from RNA-Seq data without a reference genome. *Nat. Biotechnol.* https://doi.org/10.1038/nbt.1883 (2011).
44. The UniProt Consortium, UniProt: a worldwide hub of protein knowledge. *Nucleic Acids Res.* **47**, D506–D515 (2019).
45. Camacho, C. et al. BLAST+: architecture and applications. *BMC Bioinformatics* https://doi.org/10.1186/1471-2105-10-421 (2009).
46. Love, M. I., Huber, W. & Anders, S. Moderated estimation of fold change and dispersion for RNA-seq data with DESeq2. *Genome Biol.* **15**, 550 (2014).
47. Schmidt, H. et al. A high-quality genome assembly from short and long reads for the non-biting midge *Chironomus riparius* (Diptera). *G3 (Bethesda)* https://doi.org/10.1534/g3.119.400710 (2020).
48. Rohart, F., Gautier, B., Singh, A. & Lê Cao, K.-A. mixOmics: an R package for 'omics feature selection and multiple data integration. *PLoS Comput. Biol.* https://doi.org/10.1371/journal.pcbi.1005752 (2017).
49. Chiesa, M., Colombo, G. I. & Piacentini, L. DaMiRseq—an R/Bioconductor package for data mining of RNA-Seq data: normalization, feature selection and classification. *Bioinformatics* **34**, 1416–1418 (2018).
50. Gu, Z., Eils, R. & Schlesner, M. Complex heatmaps reveal patterns and correlations in multidimensional genomic data. *Bioinformatics* **32**, 2847–2849 (2016).
51. Mi, H. et al. Protocol Update for large-scale genome and gene function analysis with the PANTHER classification system (v.14.0). *Nat. Protoc.* **14**, 703–721 (2019).
52. Raudvere, U. et al. g:Profiler: a web server for functional enrichment analysis and conversions of gene lists (2019 update). *Nucleic Acids Res.* **47**, 191–198 (2019).

Acknowledgements

This material is based upon work supported by the National Science Foundation under Grant No. CHE-2001611, the NSF Center for Sustainable Nanotechnology (R.J.H and R.D.K.). The Center for Sustainable Nanotechnology is part of the Centers for Chemical Innovation Program. This project used the UWM Great Lakes Genomics Center sequencing and bioinformatics services. UWM Institutional Animal Care and Use Committee protocols followed 20-21 no. 01 and 20-21 no. 50.

Author contributions

B.J.C., N.J.N. and R.D.K. conceived the experiment and its design. B.J.C., N.J.N. and E.B. carried out the LCO nanosheet exposures. A.S. prepared the RNA-Seq libraries. O.M. and A.A.M. conducted bioinformatic quality-control analysis and RNA-Seq data analysis. B.J.C. carried out additional downstream analyses, including PLS-DA, pathway classification and enrichment analysis. E.D.L. and R.J.H. provided nanomaterial synthesis and characterization. Y.S. and J.C.W. carried out elemental analysis. B.J.C. and R.D.K. wrote and edited the paper, with contributions and support from all co-authors. Research was supervised by R.D.K.

Competing interests

The authors declare no competing interests.

Additional information

Supplementary information The online version contains supplementary material available at https://doi.org/10.1038/s41565-022-01096-2.

Correspondence and requests for materials should be addressed to Rebecca D. Klaper.

Peer review information *Nature Nanotechnology* thanks the anonymous reviewers for their contribution to the peer review of this work.

Reprints and permissions information is available at www.nature.com/reprints.